Journal of Materials Chemistry C

ROYAL SOCIETY OF CHEMISTRY

PAPER

View Article Online
View Journal | View Issue

Cite this: J. Mater. Chem. C, 2025, 13, 177

The influence of stabiliser concentration on the formation of In_2O_3 thin films†

Aysha A. Riaz,[a] Curran Kalha,[a] Maria Basso,[b] Máté Füredi‡[c] and Anna Regoutz *[ad]

Received 22nd July 2024,
Accepted 22nd October 2024

DOI: 10.1039/d4tc03116d

rsc.li/materials-c

In_2O_3 is the parent oxide semiconductor for many transparent conducting oxides owing to its comparatively wide band gap and reasonable conductivity. The ability to fabricate thin films of In_2O_3 utilising simple and cheap solution-processed methods has made it appealing for applications in displays and solar cells. However, to optimise and improve the optoelectronic properties of these films and enable scalability, understanding the fundamentals behind the solution chemistry is essential and often overlooked. Current research highlights the use of stabilisers to maintain the solution over time and facilitate the formation of strong M–O–M bonds but rarely delves into the underlying chemistry or discusses the effect of varying the stabiliser concentration. This paper explores the impact on the quality of In_2O_3 thin films when altering the concentration of monoethanolamine used as a stabiliser. UV-visible and infrared spectroscopy are employed to track changes to the solution over time to explore the role of the stabiliser. In parallel, thin films prepared from solutions at different time points were characterised using X-ray photoelectron spectroscopy, atomic force microscopy, and ellipsometry. Through this approach, changes in the solution can be directly correlated to thin-film characteristics, crucial for their use in electronic applications.

1 Introduction

Indium oxide, In_2O_3 thin films have been extensively studied, given they are a benchmark parent system for transparent conducting oxides (TCOs) at the heart of optical and electronic devices. Particular attention has been paid to the effects of dopants on the optoelectronic properties of these TCOs.[1–4] However, of equal but often disregarded importance is the understanding of how the deposition method and film quality affects their properties. In_2O_3 thin films have been deposited by a variety of methods, including pulsed laser deposition (PLD), molecular beam epitaxy (MBE), and chemical vapour deposition (CVD) – all of which are examples of energy-intensive vacuum deposition processes.[5–7] Solution processes, particularly sol–gel approaches, have become a viable alternative to these methods as they are simple, low cost, and have the ability to coat large surfaces more easily, proving more advantageous over the often complex setups of the more established deposition methods.[8,9] Their simple nature is based on the need for only an indium-based precursor, appropriate solvent, and stabiliser without the need for a vacuum. The precursor, which is usually a metal salt or alkoxide, is dissolved in an alcoholic solvent where a slow hydrolysis process occurs to form metal hydroxides. Condensation reactions then follow where the metal hydroxides react with each other, forming a series of metal–oxygen–metal (M–O–M) bonds.[10] When the solution is deposited on a substrate and drying begins, the metal oxides (MOs) network increases further, but residual groups from the solvent or stabiliser remain. Upon annealing, the residual groups are removed, and a stable, porous metal oxide network is established.[11] The formation of a MO thin film relies on two fundamental sol–gel reactions: (I) hydrolysis and (II) condensation. For the widely used indium nitrate precursor, eqn (1) shows how aquo-ions are formed, which then undergo hydrolysis per reaction (2):

$$In(NO_3)_3{\cdot}3H_2O \xrightarrow{\text{solvation}} [In(H_2O)_3]^{3+} + 3(NO_3)^- \quad (1)$$

$$[In(H_2O)_3]^{3+} + H_2O \xrightarrow{\text{hydrolysis}} [In(OH)(H_2O)_2]^{3+} + H_3O^+. \quad (2)$$

Hydrolysis is the rate-determining step for this process and can be influenced by the pH and polarity of the M–OR bond. It is important to control the rate of hydrolysis, *e.g.* to avoid rapid

[a] Department of Chemistry, University College London, 20 Gordon Street, London WC1H 0AJ, UK. E-mail: anna.regoutz@chem.ox.ac.uk
[b] Department of Industrial Engineering, University of Padova and INSTM, Via Marzolo 9, Padova 35131, Italy
[c] Department of Chemical Engineering, University College London, Torrington Place, London, WC1E 7JE, UK
[d] Department of Chemistry, University of Oxford, Inorganic Chemistry Laboratory, South Parks Road, OX1 3QR, Oxford, UK

† Electronic supplementary information (ESI) available. See DOI: https://doi.org/10.1039/d4tc03116d

‡ Semilab Co. Ltd., Prielle Kornélia u. 2. H-1117 Budapest, Hungary.

precipitation, which has a detrimental effect on thin film quality. Therefore, stabilisers in the form of acids or bases are added. Under basic conditions, the condensation rate is higher than the hydrolysis rate, resulting in a highly branched gel.[10] This is because, under basic conditions, there are more –OH ions present rather than aqua-ions, which facilitate condensation better.[12] Alkanolamines such as monoethanolamine (MEA) or diethanolamine (DEA) are commonly used as stabilisers as they are basic and thought to have a chelating effect, which slows down the rate of hydrolysis. This hydrolysis reaction continues between indium species, eventually forming $In(OH)_3$, which then undergoes condensation through the following reaction, facilitated by heat:

$$2In(OH)_3 \xrightarrow{\Delta H} In_2O_3 + 3H_2O. \quad (3)$$

This final annealing stage is essential as residual solvent and stabiliser groups remain in the M–O–M network and must be removed. Kumaran *et al.* confirmed that metal nitrates do not fully dissociate in solution but will be removed during high-temperature annealing.[13]

Although the effects of different indium precursors and solvents have been studied, the role of the stabiliser is less explored.[13–15] The stability of the solution has been followed by observing the formation of precipitates, with the idea that the more precipitates form, the more unstable the solution is. Xu *et al.* noted that with the use of diethanolamine (DEA) precipitation occurred as a result of increased pH which drives the hydrolysis of In^{3+} to form $In(OH)_3$, however, DEA simultaneously chelates with In^{3+} which inhibits rapid hydrolysis and promotes condensation.[16] Qiu *et al.* demonstrated how the addition of MEA facilitates the formation of more M–O–M bonds, determined *via* X-ray photoelectron spectroscopy (XPS) measurements, concluding that it is essential to incorporate MEA for high-performance thin film transistors (TFTs).[17] Moreover, DEA and MEA have been studied comparatively by Winer *et al.* who highlighted how the choice of stabiliser can affect the condensation and crystallisation of the metal oxide film. As DEA contains an additional hydroxyl group, the chelating effect between the metal ions and hydroxyl groups is stronger than in MEA, causing an increase in the temperature needed to decompose organic residues and crystallise the film.[18]

Optimising the sol–gel solution is a critical step in successfully forming high-quality In_2O_3 thin films and has a direct impact on their optoelectronic properties. For example, increasing indium precursor concentration has been shown to result in denser films that have lower mobility.[19] This study goes beyond the current literature to examine how the amount of a widely used stabiliser, MEA, affects the solution across a 48-hour time period, during which significant changes occur. It establishes the long-term stability of the solution, which is essential for industrial applications and improving sustainability. Furthermore, the effect of stabiliser to precursor ratio is investigated to achieve improved methods for depositing films of In_2O_3 and better application properties in devices. Understanding the stability of the solution extends its usage, thus minimising waste, conserving materials and proving advantageous for industry scale-up. UV-vis and infrared (IR) spectroscopy are used to monitor the changes in the amount of precipitate and chemical changes occurring in the solution. Additionally, films are deposited across the same time period, and XPS provides an understanding of the changing film chemistry before annealing and depending on solution make-up. Resulting annealed films are further studied using atomic force microscopy (AFM), ellipsometry, and XPS to establish effects on the final In_2O_3 film properties relevant for electronic device applications.

2 Methods

2.1 Sol–gel solution preparation

A 0.1 M sol–gel solution of In_2O_3 was prepared by dissolving indium nitrate hydrate, $In(NO_3)_3{\cdot}3H_2O$ (99.9%, Sigma-Aldrich, CAS: 207398-97-8) in 2-methoxyethanol (≥99.3%, Sigma-Aldrich, CAS: 109-86-4) in a 25 mL beaker at room temperature (20 °C). Monoethanolamine (MEA, ≥99%, Sigma-Aldrich, CAS: 141-43-5) was added to the solution using an Eppendorf pipette, with the molar ratio of MEA : In being varied from 0 : 1 to 1 : 1. The solution was subsequently allowed to stir at 600 rpm for one hour. In between depositions, the beaker was covered with parafilm.

2.2 Film deposition

Substrates were cut from silicon wafers with native oxide into approximately 10 × 10 mm^2 square pieces using a diamond-tipped pen. They were then rinsed with deionised (DI) water, followed by propan-2-ol and dried with nitrogen gas. Finally, a Novascan PSD UV/ozone lamp was used to treat the substrates for 30 min. A Nadtech ND-DC 11/1 300 dip coater was used to produce thin films. The 25 mL beaker of the prepared In_2O_3 sol–gel solution was placed in the sample chamber where the cleaned substrate was held above by stainless steel crossover tweezers. The substrates were immersed at a speed of 50 mm min^{-1} and held for 20 s. They were then withdrawn at a speed of 5 mm min^{-1} and allowed to dry in air. Samples were deposited at varying times relative to the completion of stirring and dipped only once to ensure consistency over deposition timing. One set of thin films, referred to as 'Annealed', were deposited 4 hours after stirring, then transferred to an alumina boat upon completion of dip-coating, and inserted into an Elite standard horizontal single zone tube furnace controlled by a Eurotherm type 3216cc digital PID controller where they were heated to 400 °C at a heating rate of 5° min^{-1} for two hours in air. They were then allowed to cool to room temperature without active cooling.

2.3 Collection of precipitates

For all solutions except those without stabiliser, some precipitates formed, which settled to the bottom of the beaker. These were separated by 10 min centrifugation with a Sigma 2-16KL centrifuge at 5000 rpm. The liquid was decanted, and the

resulting white gel was extracted. The gel was dried in a desiccator for up to 72 h until completely dry and in powder form.

2.4 Characterisation

The sol–gel solutions were analysed by UV-vis spectroscopy using a Shimadzu 2700i UV-vis spectrophotometer with a double monochromator system. The light sources were a tungsten lamp (350–800 nm), which switched to a deuterium lamp (200–350 nm) at approximately 350 nm. Solutions were measured in Fisherbrand Polystyrene Macro Cuvettes with 2-methoxyethanol as the reference. Measurements were collected over a range of 230 to 600 nm with a step size of 2 nm. Complementary Fourier transform infrared (FTIR) spectra were recorded on the solutions on an attenuated total reflectance (ATR) spectrometer by Shimadzu between 4000–450 cm^{-1}.

Thin films of In_2O_3 were characterised by XPS using a laboratory-based Thermo Scientific K-Alpha spectrometer equipped with a monochromated Al Kα source ($h\nu$ = 1486.7 eV) and a 180° double focusing hemispherical analyser. All spectra were collected with a flood gun at 100 μA to reduce excessive charging and with the maximum X-ray spot size of 400 μm to optimise the efficiency of collecting high-resolution spectra. 20 and 200 eV pass energies were used for the collection of core level and survey spectra, respectively. Data processing of the spectra was performed using the Thermo Avantage v5.9925 software package. A Semilab SE-2000 spectroscopic ellipsometer with a xenon lamp as a light source and adjustable arms and stage was used to obtain film thicknesses. The analyser arm contains a rotating compensator and both UV-vis and NIR detectors. Data were collected across three angles (60°, 70°, and 75°) between 0.8 and 4.4 eV photon energy. SEA software was used to fit the data with the Sellmeier and Lorentz dispersion laws. The dispersion law parameters were kept constant across all samples. Thin-film grazing incidence X-ray diffraction (GI-XRD) was carried out using a Panalytical Empyrean diffractometer with a monochromated Cu Kα source ($K\alpha_1$ and $K\alpha_2$, λ = 1.540598 and 1.544426 Å, respectively) operated at 40 kV with 40 mA emission current. Grazing incidence measurements were taken with the incident beam angle (ω) set at 0.5°, and a 2θ range of 20–80° was measured with a step size of 0.1° at 4 s per step.

Finally, AFM data were collected by an Agilent 5500 AFM in AC AFM mode with a scan speed of 0.5 lines per s. Silicon AFM probes (NuNano Ltd, 18 N m^{-1} spring constant) were used. The WSxM 5.0 software was used to process images and calculate root mean square (RMS) values in nm. The RMS values were determined based on an average of three images of different sample areas per sample.[20]

3 Results and discussion

Four ratios of stabiliser to indium were selected (1 : 1, 0.50 : 1, 0.25 : 1 and 0 : 1), and the transmittance of each solution was followed by UV-vis spectroscopy at time intervals of 0, 2, 24, and 48 h after stirring in air. At time 0 h, the solutions containing the stabiliser show minimum transmittance across the UV-vis range, which then gradually increases up until 24 h, as shown in Fig. 1.

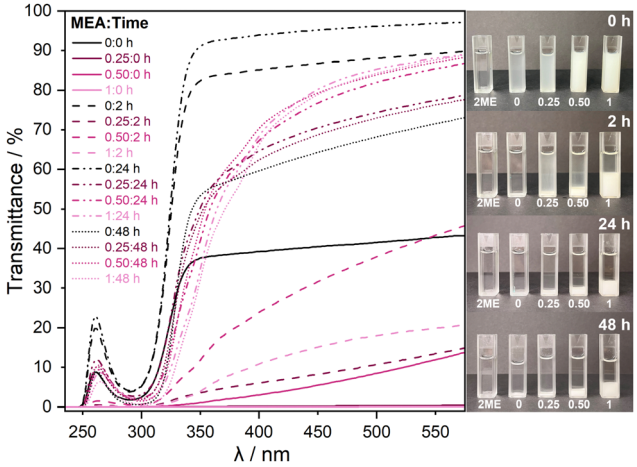

Fig. 1 UV-vis transmittance (left) and photographs of the corresponding solutions (right) for four MEA stabiliser : In ratios including 1 : 1, 0.50 : 1, 0.25 : 1, and 0 : 1. The photos on the right show the ageing solutions (left to right: from lowest to highest ratio) across the 48 h time period.

At 48 h, there is a slight drop in transmittance due to the formed precipitates settling at the bottom of the solution, as is clearly visible in the images on the right in Fig. 1. The nature of the precipitates is discussed later. Additionally, Fig. S1 in the ESI† displays the changes in precipitates from the original beakers. Xu *et al.* observed comparable behaviour upon the addition of an ethanolamine stabiliser.[16] Between 24 h and 48 h, the solution settles, and there is very little further change. Therefore, data was not collected beyond 24 h for other techniques. The solution with no stabiliser does not form visible precipitates, resulting in a higher overall transmittance. The minimum in transmittance at approximately 280 nm is attributed to absorption from nitrate ions originating from the precursor.[13] Fig. S2 in the ESI† shows the nitrate absorption in more detail, exhibiting increased absorption between 0 and 2 h, later confirmed by XPS. In the initial two hours, there is more solvation of precursor, which is then hydrolysed, thus reducing the presence of nitrates. Furthermore, there is a shift to lower wavelengths for the solution without stabiliser, which can be explained by nitrate groups that do not associate entirely, which Kumaran *et al.* also observed.[13]

IR data in Fig. 2 follow the changes in the solution of each stabiliser ratio between 0 and 24 hours. Contributions from the reference solvent measurements have been subtracted from the overall spectra to aid interpretation of key changes, *e.g.* in the In species. It would be expected that a gradual increase in In–O environments (between 410–500 cm^{-1}) is observed as the nitrate is hydrolysed over time.[21] Although it is difficult to distinguish between In–O and In–OH environments, it can be inferred through the increase in the O–H environments (at 1650 and 3235 cm^{-1}) over time that $In(OH)_3$ is being formed.[22] The solution with no stabiliser has the biggest increase in O–H, suggesting faster hydrolysis of the nitrate species without stabiliser and that in all other samples In may be coordinated with the stabiliser instead.

The N–O environments at 1298 and 1516 cm^{-1} show a small decrease over time as they are being hydrolysed. This is

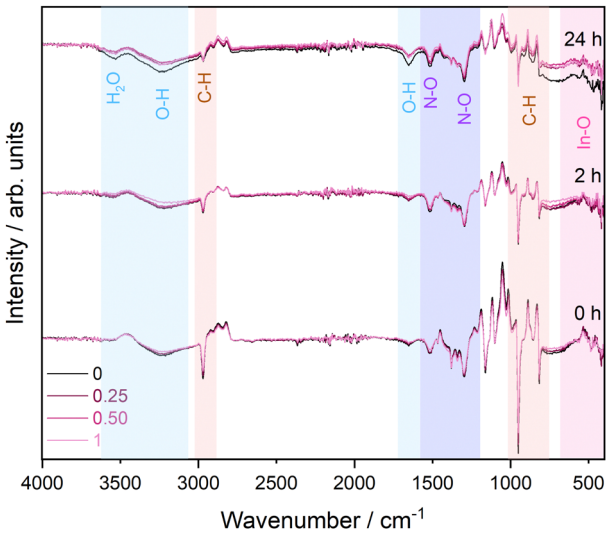

Fig. 2 Stacked infrared spectra in the 500–4000 cm^{-1} region for all four solution ratios from 0–24 hours after subtraction of a solvent reference spectrum.

consistent with the decrease of nitrate observed in the UV-vis. Additionally, there is a noticeable decrease in C–H environments (816–986 and 2968 cm^{-1}) over time. Fig. S3 (ESI†) shows the stabiliser is undetectable by IR, given its low concentrations, and no signal from amine groups is visible in the IR spectra. The C–H groups observed originate from the solvent. The associated wavenumbers and assignments of the main peaks are summarised in Table S1 in the ESI.† Whilst a solvent reference has been subtracted from the spectra, the peaks visible here somewhat shift in wave number due to interaction with the precursor and stabiliser. Over time, the C–H signals decrease significantly as they begin to overlap more strongly with the solvent reference, indicating that the sol–gel solution is becoming more and more dominated by the solvent as the formation of precipitates progresses and settles.[23] An enlarged view of the C–H feature can be found in Fig. S4 in the ESI.† IR data were also collected for the precipitates extracted from the solutions after 24 hours, which are shown in Fig. S5 in the ESI,† exhibiting signals commensurate with the presence of a mixture of In–OH environments and nitrate species.

To further explore the nature of the precipitates forming and to follow the chemical changes occurring in the solution, the formed precipitates and thin films of each solution deposited at time intervals of 0, 2 and 24 hours were measured using XPS. The XPS spectra for the precipitates, shown in Fig. S6 in the ESI,† indicate a mixture of hydroxide and oxide environments, with some nitrate present, in agreement with the IR results. From the survey spectra of the thin films deposited from each of the four ratios after 24 hours, found in Fig. S7 in the ESI,† all expected elements, In, O, N and C, were detected. In addition, trace levels of Cl and Mg, which are attributed to impurities deposited on the surface during sample preparation, were present. Fig. 3 shows selected core level spectra collected from films deposited from each of the four ratios after 24 hours, as these show the most distinct variations. The complete core state dataset, including all ratios and times, is shown in Fig. S8 in the ESI.†

The In 3d spectra shown in Fig. 3(a) show a spin–orbit splitting (SOS) of 7.6 eV with the In $3d_{5/2}$ peaks at a binding energy (BE) of 445.0 eV consistent with In–OH/In–MEA environments.[8] Only in the 0 : 1 ratio is a slight difference in peak width and position observed, indicating the presence of small amounts of In_2O_3.[24] These differences between films are evident in the O 1s spectra (see Fig. 3(b)) and peak fit analysis was performed to extract the peak positions of individual chemical states (see Fig. S9 in the ESI† for a representative peak fit of the O 1s core level spectrum). The O 1s spectra show a clear peak at 530.5 eV associated with an In–O metal lattice oxide environment for the 0 : 1 and 0.25 : 1 ratios. In general, metal oxide peaks are observed at 530 ± 0.5 eV. Peaks visible in the other two samples at 531.2 and 532.1 eV can be assigned to hydroxyl and SiO_2 species, respectively,[25,26] with the SiO_2 signal originating from the substrate. Given that the probing depth of

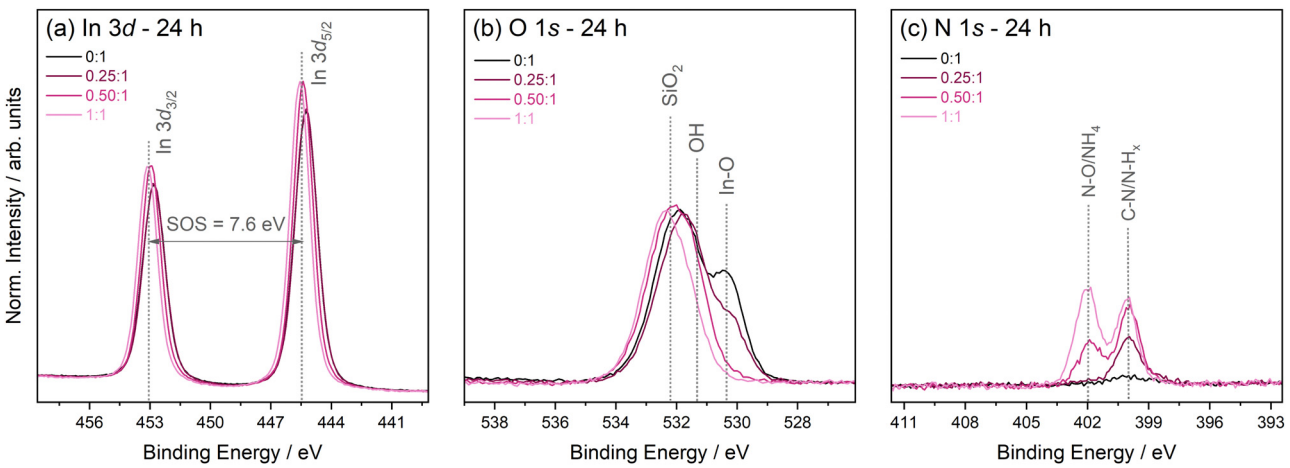

Fig. 3 XPS core level spectra, including (a) In 3d, (b) O 1s, and (c) N 1s, for each stabiliser ratio after 24 hours. Spectra are normalised to the respective areas of the In $3d_{5/2}$ peak.

XPS for the O 1s line using the Al Kα excitation energy is approximately 7 nm (the relativistic inelastic mean free path for In_2O_3 was calculated using the QUASES-IMFP-TPP2M software package with the band gap value entered as 2.9 eV),[27] the observation of a Si–O environment indicates that the films are incredibly thin or discontinuous, which is expected as only a single coat was applied. The N 1s spectra (see Fig. 3(c)) exhibit environments associated with the amine group from MEA and the breakdown of nitrate from the precursor.[28] Fig. 4 shows the overall rel. at% of N increasing with increasing stabiliser amount relative to In content. The rel. at% of C follows a similar trend suggesting the C also originates from the MEA. Overall, with less stabiliser in the solution, there is less oxide formation after 24 hours. Over time, MEA chelates with In atoms and reduces the premature formation of any oxide.

In addition to as-deposited, unannealed thin films, an annealed thin film was prepared for each stabiliser ratio after 4 hours to understand the effects of annealing and the make-up of the final In_2O_3 films. Fig. S10 in the ESI† compares the survey spectra of these films with films extracted from the 0.50 : 1 ratio solution aged from 0 to 24 hours. Again, all expected elements, In, O, N and C, were detected. Fig. 5 shows the selected core level spectra from this series, including In 3d, O 1s and N 1s.

Here, the In $3d_{5/2}$ peak (see Fig. 5(a)) for the as-deposited films is at a BE of 445.0 eV consistent with In–OH/In–MEA environments. There is a distinct change in peak position and width for the annealed film. The peak moves to a lower BE of 444.1 eV and has an asymmetric shape typical of an In_2O_3 film.[8] The asymmetry of the peak is associated with lifetime effects causing the broadening of the higher BE peak as both an unscreened and screened final state are possible in In_2O_3.[24] The O 1s spectra (see Fig. 5(b)) confirm the conversion from In–OH/In–MEA to an oxide during annealing, with the appearance of a strong peak at 530.0 eV commensurate with lattice oxygen of In_2O_3. After 2 h, a slight increase in In–OH/In–MEA environments is observed (peak at 531.0 eV), reducing greatly after 24 h. This can be explained by the increasing amount of precipitate forming with increasing stabiliser amount, as the addition of MEA, which is basic, results in a higher pH. This not only facilitates hydrolysis of the nitrate but also causes hydroxide and oxide to precipitate out of the solution.[29] The solution with no stabiliser remains clear throughout, as hydroxide and oxide do not precipitate at lower pH. As noticed in the UV-vis experiment, there is an increase in transmittance of the solution at 24 hours, a consequence of the precipitate settling to the bottom of the solution. Given that the precipitate is a mixture of oxide and hydroxide, as mentioned earlier, this partially explains why a drop in In–OH is observed. However, understanding the chelating nature of the stabiliser helps to explain this observation fully. Over time, MEA can chelate with the In atom and reduce the premature formation of any oxide.[18] The N 1s spectra (see Fig. 5(c)) show comparable chemical environments as the 24 h dataset discussed above. In addition, minute NO_3 signals originating from the precursor are visible between 0 and 2 h as the solution is still undergoing hydrolysis. The peak labelled with an asterisk at 398.6 eV is thought to be a reduced N–H group formed due to radiation effects during XPS measurements from the reduction of N–O environments.[28,30] Hence explaining why no N–H environments were observed in the IR data. The annealed film shows removal of N, in parallel with a strong reduction of the carbon content (see Fig. 4), confirming the successful conversion of the gel network to metal oxide and the removal of any remaining stabiliser and solvent.

Regardless of the stabiliser concentration used, all solutions can form In_2O_3 films, although with varying quality. Quantifying the ratio of hydroxide to oxide in the thin films is an important indicator of film quality, as any remaining hydroxide can diminish final device performance. Table 1 compares the hydroxide and oxide amounts for each annealed film. The solution with a 0.50 : 1 ratio produced the film with the lowest hydroxide contribution, but due to the complex interactions of the stabiliser with the sol–gel formation, there is no simple, overall trend detectable. Qiu *et al.* concluded similar results of no discernible trend but agreed that adding MEA improved the hydroxide-to-oxide ratio, resulting in improved electrical properties.[17] A full quantitative analysis of the hydroxide to oxide ratios for all samples, including the as-deposited films, are shown in Table S2 of the ESI.†

This result contributes to the idea that finding a balance between precursor and MEA addition is crucial, as although MEA can control the hydrolysis through chelating, too much can cause the opposite effect due to the increase in pH.[16] This is further emphasised by a clear reduction in film thickness deposited with increasing stabiliser concentration (see Table 1 for thicknesses determined from ellipsometry. The corresponding fits are shown in Fig. S11 in the ESI†). Due to the ultra-thin nature of the film, the structure and crystallinity of the film could not be confirmed using XRD. However, a thicker sample was made using the same solution and ratio of 0.50 : 1 but with 13 dip cycles, resulting in a diffraction pattern commensurate with polycrystalline In_2O_3 in the bixbyite structure (see Fig. S12 in the ESI†).

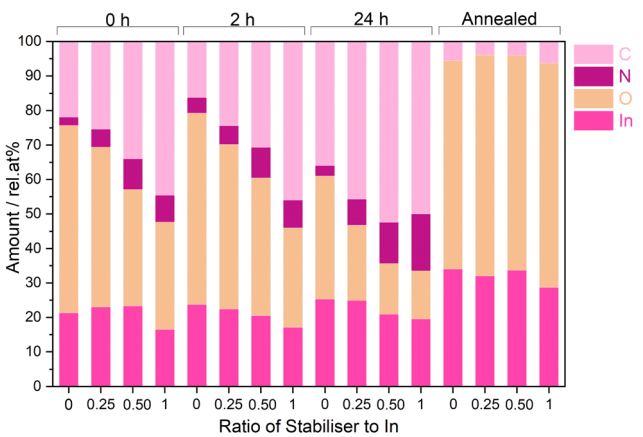

Fig. 4 Comparison of the relative atomic% of C, N, O and In in as-deposited and annealed films of each stabiliser ratio across the 24 hours.

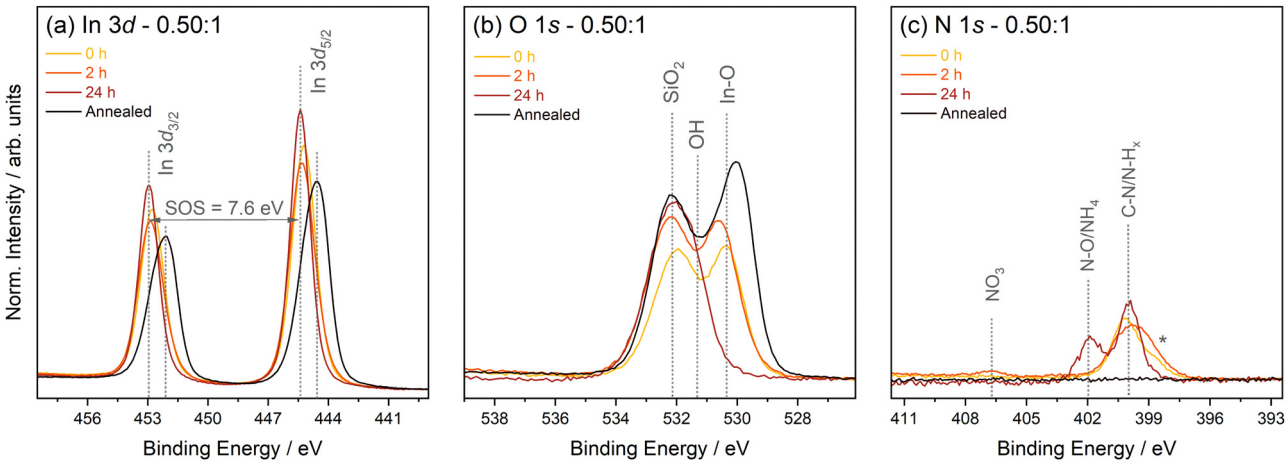

Fig. 5 XPS core level spectra, including (a) In 3d, (b) O 1s, and (c) N 1s, for the stabiliser ratio 0.50 : 1 between 0–24 hours and including the annealed film. Spectra are normalised to the respective areas of the In $3d_{5/2}$ peak.

Table 1 Table listing the relative atomic% of $In(OH)_3$ and In_2O_3 from XPS present for the four annealed films with varying stabiliser amounts, as well as corresponding thicknesses *d* obtained by ellipsometry

Stabiliser ratio	$In(OH)_3$ (rel. at%)	In_2O_3 (rel. at%)	*d* (nm)
0 : 1	30.1	69.9	5.0
0.25 : 1	34.0	66.0	4.9
0.50 : 1	28.8	71.2	4.7
1 : 1	37.6	62.4	3.7

Following the exploration of the chemical nature of the deposited films, AFM was used to understand how the stabiliser concentration affects their morphology and roughness. Fig. 6 shows AFM images of the four annealed In_2O_3 films with calculated RMS roughness values in nm. Overall, increasing the amount of stabiliser increases the film's roughness and a change in the morphology is observed. The roughness is more than three times as high when a 1 : 1 ratio is used compared to a film without stabiliser. Qiu *et al.* observed similar roughness values when varying MEA concentrations, however, they found the film without stabiliser to have the highest roughness.[17] Furthermore, the morphology changes from a very flat film to the formation of distinct circular features on the film surface. Jiaxiang *et al.* and Xu *et al.* also observed improved particle sphericity with the addition of MEA.[16,31] However, at the highest stabiliser concentration, there is formation of large gaps. The excess stabiliser leads to increased hydroxide/oxide precipitation, which affects the formation of a homogenous M–O–M framework and, in turn, affects the formation of homogeneous thin films. An additional risk of higher MEA addition is that through the increase in chelation of MEA with In ions, more MEA remains in the thin films, as seen in XPS through the increase of a C–N environment at high concentrations of stabiliser, resulting in a greater chance of cracking of the film occurring during thermal annealing.

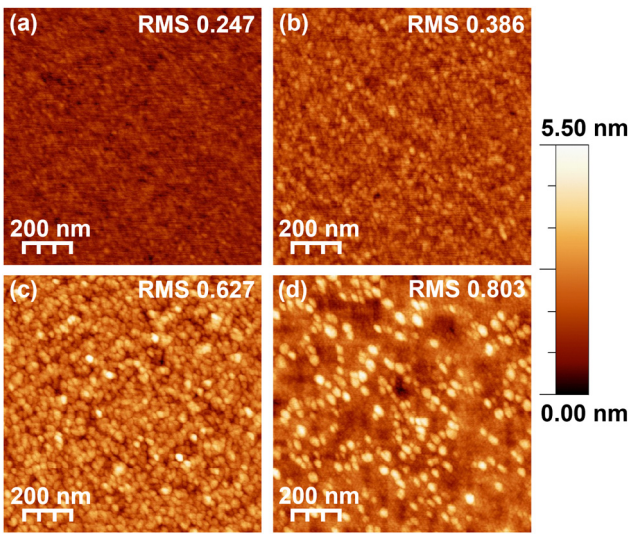

Fig. 6 AFM images (1 × 1 μm^2) of the four annealed In_2O_3 films with varying stabiliser concentrations: (a) 0, (b) 0.25, (c) 0.50 and (d) 1. The corresponding RMS values in nm are shown in the upper right corner of each image. All images are shown over the same height range.

4 Conclusions

This work investigates the effect of altering the stabiliser concentration on the deposition of In_2O_3 thin films from sol–gel by following the characteristics of the ageing solution and the resulting films. It concludes that without stabiliser, rapid oxide formation occurs in solution but slows considerably with the addition of more stabiliser due to chelating effects decreasing the hydrolysis rate. This allows the solution to remain usable for an extended period of time, which is important for scaling to continuous film deposition. With increasing stabiliser amount, a larger amount of In–OH/In–MEA species precipitate due to the increase in pH, causing cloudiness in the solution as quantified through transmittance UV-vis spectroscopy. However, precipitates or cloudiness are not necessarily detrimental to the formation of In_2O_3, with all solutions

forming In_2O_3 of acceptable purity. The hydroxide contribution varies with stabiliser concentration, and the 0.50 : 1 ratio of MEA : In resulted in the lowest hydroxide presence. AFM revealed the strong dependency of roughness and film homogeneity on the stabiliser concentration, with films becoming much rougher when the stabiliser amount increases.

This work clearly demonstrates that the ratio of precursor and stabiliser has to be chosen carefully, and a balance must be achieved between the stabiliser controlling hydrolysis and, at the same time, avoiding rapid precipitate formation. However, it also shows that it is not essential to produce completely clear solutions devoid of any precipitation. The 0.50 : 1 ratio of MEA : In proved to be optimal overall for the preparation of In_2O_3 films, but this ratio is often not defined in the literature. Only one other study found similar results using a 1 : 1 molar ratio of stabiliser to In, however, DEA and $InCl_3$ were used instead of the present sol–gel recipe.[16] Work by Qiu *et al.* investigated higher concentrations of MEA but agreed there was a limitation on improving the film qualities through using MEA. Almost all other research emphasises the formation of clear solutions, but there is no investigation of the nature of the precipitates. Furthermore, there are limited studies understanding how the stabiliser concentration affects the long term stability of the solution. In this work, a deeper understanding of the long-term stability and stabiliser interaction with the solution can be applied for future work with alternative precursors and solvents to optimise the deposition of oxide thin films and improve device performance.

Data availability

Data for this article, including all processed data of the main paper figures, are available at Zenodo at [**https://doi.org/10.5281/zenodo.12706179**] in Origin format.

Conflicts of interest

There are no conflicts to declare.

Acknowledgements

AAR and CK acknowledges the support from the Department of Chemistry UCL. AR acknowledges the support from the Analytical Chemistry Trust Fund for her CAMS-UK Fellowship. The authors would like to thank Prajna Bhatt, Nathalie Fernando, and Yujiang Zhu for their training and fruitful discussions.

Notes and references

1 A. Regoutz, R. G. Egdell, D. J. Morgan, R. G. Palgrave, H. Téllez, S. J. Skinner, D. J. Payne, G. W. Watson and D. O. Scanlon, *Appl. Surf. Sci.*, 2015, **349**, 970–982.
2 J. E. N. Swallow, B. A. D. Williamson, B. Sanjayan Sathasivam, M. Birkett, T. J. Featherstone, P. A. E. Murgatroyd, H. J. Edwards, Z. W. Lebens-Higgins, D. A. Duncan, M. Farnworth, P. Warren, N. Peng, T.-L. Lee, L. F. J. Piper, A. Regoutz, C. J. Carmalt, I. P. Parkin, V. R. Dhanak, D. O. Scanlon and T. D. Veal, *Mater. Horiz.*, 2020, **7**, 236.
3 O. Bierwagen, *Semicond. Sci. Technol.*, 2015, **30**, 24001.
4 D. Yao, X. Xiong, X. Fu, Z. Xu, H. Ning, D. Luo, H. Tang, H. Zheng, R. Yao and J. Peng, *Surf. Interfaces*, 2021, **27**, 101459.
5 Z. Chen, K. Saito, T. Tanaka and Q. Guo, *Thin Solid Films*, 2022, **756**, 139383.
6 A. Bourlange, D. J. Payne, R. G. Palgrave, J. S. Foord, R. G. Egdell, R. M. Jacobs, A. Schertel, J. L. Hutchison and P. J. Dobson, *Thin Solid Films*, 2009, **517**, 4286–4294.
7 C. E. Knapp, A. Kafizas, I. P. Parkin and C. J. Carmalt, *J. Mater. Chem.*, 2011, **21**, 12644–12649.
8 N. M. Twyman, K. Tetzner, T. D. Anthopoulos, D. J. Payne and A. Regoutz, *Appl. Surf. Sci.*, 2019, **479**, 974–979.
9 S. A. Palomares-Sanchez, B. E. Watts, D. Klimm, A. Baraldi, A. Parisini, S. Vantaggio and R. Fornari, *Thin Solid Films*, 2018, **645**, 383–390.
10 D. Loncarevic and Z. Cupic, *Industrial Applications of Nanomaterials*, 2019, pp. 91–122.
11 Y.-H. Kim, J.-S. Heo, T.-H. Kim, S. Park, M.-H. Yoon, J. Kim, M. S. Oh, G.-R. Yi, Y.-Y. Noh and S. K. Park, *Nature*, 2012, **489**, 128–132.
12 C. J. Brinker and G. W. Scherer, *Sol-Gel Science: The Physics and Chemistry of Sol-Gel Processing*, 2013, pp. 20–95.
13 S. Kumaran, M.-T. Liu, K.-Y. Lee and Y. Tai, *Adv. Eng. Mater.*, 2019, **22**, 1901053.
14 L. G. Bloor, C. J. Carmalt and D. Pugh, *Coord. Chem. Rev.*, 2011, **255**, 1293–1318.
15 R. M. Pasquarelli, D. S. Ginley and R. OHayre, *Chem. Soc. Rev.*, 2011, **40**, 5406–5441.
16 X. Q. Xu, Y. Zhang and G. Xu, *Mater. Sci. Forum*, 2009, **610**, 610–613.
17 H. Qiu, H. Sun, L. Zheng, J. Xiao and H. Zhou, 2021 9th International Symposium on Next Generation Electronics (ISNE), 2021, pp. 1–3.
18 I. Winer, G. E. Shter, M. Mann-Lahav and G. S. Grader, *Mater. Res.*, 2011, **26**, 1309–1315.
19 L. N. Lau, N. B. Ibrahim and H. Baqiah, *Appl. Surf. Sci.*, 2015, **345**, 355–359.
20 I. Horcas, R. Fernández, J. M. Gómez-Rodríguez, J. Colchero, J. Gómez-Herrero and A. M. Baro, *Rev. Sci. Instrum.*, 2007, **78**, 13705.
21 M. Jothibas, C. Manoharan, S. Ramalingam, S. Dhanapandian, S. Johnson Jeyakumar and M. Bououdina, *J. Mol. Struct.*, 2013, **1049**, 239–249.
22 M. I. Ivanovskaya, E. A. Ovodok and D. A. Kotsikau, *Glass Phys. Chem.*, 2011, **37**, 560–567.
23 S. Ryeon Ryu, I. Noda and Y. Mee Jung, *Appl. Spectrosc.*, 2010, **64**, 1017–1021.
24 C. Körber, V. Krishnakumar, A. Klein, G. Panaccione, P. Torelli, A. Walsh, J. L. Da Silva, S. H. Wei, R. G. Egdell and D. J. Payne, *Phys. Rev. B: Condens. Matter Mater. Phys.*, 2010, **81**, 165207.
25 I. N. Reddy, C. V. Reddy, M. Cho, J. Shim and D. Kim, *Mater. Res. Express*, 2017, **4**, 086406.

26 D. S. Jensen, S. S. Kanyal, N. Madaan, M. A. Vail, A. E. Dadson, M. H. Engelhard and M. R. Linford, *Surf. Sci. Spectra*, 2013, **20**, 36–42.
27 H. Shinotsuka, S. Tanuma, C. J. Powell and D. R. Penn, *Surf. Interface Anal.*, 2015, **47**, 871–888.
28 A. Regoutz, M. Swolinska, N. K. Fernando and L. E. Ratcliff, *Electron. Struct.*, 2020, **2**, 044005.
29 T. Sato, *J. Therm. Anal. Calorim.*, 2005, **82**, 775–782.
30 Y. Zubavichus, M. Zharnikov, A. Shaporenko, O. Fuchs, L. Weinhardt, C. Heske, E. Umbach, J. D. Denlinger and M. Grunze, *J. Phys. Chem. A*, 2004, **108**, 4557–4565.
31 L. Jiaxiang, W. U. Da, N. Zhang and W. Yue, *Rare Met.*, 2010, **29**, 143.